DISLOCATION EMISSION RENDERS PLATE-REINFORCED METAL-MATRIX COMPOSITES SUPERIOR TO SPHERICAL AND FIBROUS REINFORCEMENTS

Zhibo Zhanng[1] and Herbert M. Urbassek[2]

Physics Department and Research Center OPTIMAS, University Kaiserslautern,
Erwin-Schroedinger-Straße, D-67663 Kaiserslautern, Germany
[1] zhangzhibo5@gmail.com
[2] urbassek@rhrk.uni-kl.de; URL: http://www.physik.uni-kl.de/urbassek/
Keywords: Metal matrix composites, dislocations, reinforcements, strengthening and toughening mechanisms, atomistic simulation

ABSTRACT

Using molecular dynamics simulation, we study nanoindentation into Al/Si metal-matrix composites. Three different geometries of the Si reinforcement are considered: a spherical particle, a cylindrical fiber, and a plate. We show that plate reinforcements may absorb dislocations and emit them back into the matrix with altered glide direction, both strengthening and toughening the composite, in agreement to experiment. This mechanism does not work for spherical reinforcements, since the curved interface does not allow for dislocation emission; the case of fiber is intermediate. It is concluded that the shape of the reinforcement plays a dominant role in the mechanisms underlying the strengthening of metal-matrix composites.

1 INTRODUCTION

Metal-matrix composites (MMCs) constitute a popular class of materials with promising advantages over unreinforced metals and other composites such as polymer-matrix composites. In their recent monograph [1], Chawla and Chawla list an impressive series of improved properties of MMCs, ranging from mechanical properties over high temperature capabilities to cyclic-fatigue characteristics. In the context of the present work, the higher strength and stiffness of MMCs as compared to the unreinforced metal are particularly important.

In an MMC, the reinforcements are distributed in the form of particles [2], fibers [3], or plates [4] in the metallic matrix [1]. However, due to the incorporation of particulates and fibrous reinforcements, MMCs usually exhibit a lower ductility and toughness, and thus have a lower damage tolerance, than monolithic metals and alloys [5–7]; this feature constitutes an obvious drawback in practical application. Thus, a strategy to tailor the structure of MMCs that might endow such materials with both high strength and good ductility is in great demand.

Recently, a new type of nanoscale-laminate MMCs, developed by controlling the two-dimensional distribution of the particulate [8, 9] and fibrous [10–12] reinforcements, has become a prevailing model for developing a new generation of high-strength MMCs with considerable ductility, due to their remarkable abilities of energy absorption and dislocation storage. Similarly, graphene as plate reinforcement shows excellent mechanical properties including increased stiffness, tensile strength, total elongation under stress and toughness [13–17]. Interestingly, the strengthening and stiffening efficiency of plate/Al composites is considerably higher than that of conventional particle and fiber reinforcements [16].

Therefore, plate reinforcements are supposed to show a superior performance during the deformation of MMCs as compared to those in the form of fibers and particles [16]. However, until now, there is no comparative study to explain this relevant phenomenon. While previous experimental studies attribute the strengthening mechanism to stress transfer and dislocation hindering, and the toughening mechanism mainly to crack evolution, limitations in experiments did not permit to provide sufficient details as to the nature of these mechanisms [18, 19]. We conclude that the origin of the superiority of plate-reinforced MMCs is not clear.

Nanoindentation is a routine technique for testing the mechanical behavior of materials [20, 21]. It provides in particular information on the material hardness, and hence on the plastic deformations that can occur in it. While many aspects of the plastic behavior of elemental and homogeneous materials are understood, the response of composite materials to nanoindentation has been investigated less frequently and few experimental [22–25] or modelling [26–29] studies have been published up to now.

Molecular dynamics (MD) simulations are often used to study the atomistic processes occurring during nanoindentation in materials [30]. When applied to single crystals, MD gives results in good agreement with experiment [30, 31]. In addition, due to the versatility of computer simulation, the influence of materials properties on the indentation can readily be investigated [32, 33].

Nanomachining and in particular nanoindentation studies are performed increasingly often using molecular dynamics (MD) simulations [30]. These need only the interatomic interaction potentials as input into the simulation; thus the results obtained are essentially as good as the potentials used. The reliability of such potentials has been investigated in many cases, in particular for fcc [34], bcc [35, 36], and hcp [37] metals, but also in Si [38, 39].

In this paper, we investigate the plastic deformation behavior for the specific case of an Al/Si composite under indentation. By choosing three exemplary geometries for the Si reinforcement – a plate, a spherical particle, and a cylindrical fiber – we can shed light on the mechanisms that make the mechanical performance of plate MMCs superior to the other reinforcement geometries. Our results show that all the reinforcements in the three different shapes can deflect the gliding direction of Al dislocations; however, only the plate reinforcement is able to emit dislocations into the Al matrix. These interactions between Al dislocations and the Al/Si interfaces are in agreement with experimental studies [16]. The emission of dislocations that we observe here for the first time make plate reinforcements superior to the other two by both strengthening (higher dislocation density) and toughening (uniform and abundant plastic deformation) the matrix.

2 METHOD

We study indentation of an MMC based on fcc Al as matrix and cubic diamond Si as the reinforcement material. The simulation box has a depth of 44.5 nm and a lateral extension of 57.1 nm. The Al matrix is single-crystalline; its free surface has a (100) orientation. As shown in Figs. 1(a)–(c), three different shapes of the Si reinforcement are studied:

1. a spherical particle of radius R = 16 nm;
2. a cylindrical fiber of radius R = 16 nm;
3. a plate of thickness d = 5.4 nm beneath the Al matrix overlayer of 11.5 nm thickness.

In all three cases the thickness of Al on top of the Si reinforcement amounts to 11.5 nm, and the embedded Si particles are situated such that they touch the bottom of the simulation box. This arrangement helps to create analogous indentation scenarios in which the indenter moves only through the pure Al matrix, but the plasticity generated in the Al interacts with the Si reinforcement. The Si reinforcements are oriented such that their [100] direction is aligned with the Al [100] direction. We introduce a cartesian coordinate system centered in the middle of the top surface aligned with the cubic axes of the Al (and Si) crystals; the z axis points in the direction normal to the surface and the x axis points along the cylinder axis, see Fig. 1.

Since Al and Si have different lattice constants – 4.05 and 5.43 °A, respectively – the assemblage of the Si and Al parts to the composite structure has to be done with care. We follow the recipe of Noreyan et al. [40] and choose the lateral sizes of the interface such that they are commensurate for both the Al and Si lattices. Thus, for instance, the lateral extension of 57.1 nm can be filled by 105 lattice constants of Si and by 141 lattice constants of Al.

Before starting the simulations, the systems are relaxed such that all components of the stress tensor reach values <12 MPa, when averaged over the entire specimen, and the temperature drops below 1 K. The relaxation is performed in several steps: first an energy minimization algorithm is applied relaxing the system with periodic boundary conditions in both lateral directions. The bottom of the system (width of 1nm) is fixed in all the substrates in order to prevent any rigid-body motion of the substrate during the indentation process. The next 1nm layers at the bottom as well as the outermost 1nm layers at the sides of the substrate are thermostatted to 0 K using a velocity-scaling algorithm.

Figs. 1(d)–(f) shows the hydrostatic stress distribution in the Al/Si interfaces. Due to the large lattice mismatch of matrix and reinforcement, local (atomic) stress patterns build up. Since the global stress has been minimized, areas of positive (compressive) and negative (tensile) stress alternate in the form of a two-dimensional superlattice for the plate reinforcement, Fig. 1(d), and in the form of rings centered on the {111} facets for the spherical reinforcement Fig. 1(e). For the cylindrical fiber, both patterns are superposed.

The interactions between atoms in these three systems are described by the Al-Si potential developed by Saidi et al. [41]. They modified the Stillinger-Weber potential [42] of Si to obtain a more accurate description of the phase transformation behavior, and then combined it with the embedded-atom-model (EAM) description of pure Al developed by Mendelev et al. [43]. The combined potential is of the angular EAM type.

The indenter is positioned centrally on the top surface. It is formed as a sphere with a radius of 6 nm. Upon loading, the indenter moves perpendicularly down into the surface to a final depth of d = 6 nm with a velocity of 20 m/s. According to the recipe of Kelchner et al. [44], the interaction between an atom and the indenter is purely repulsive and follows the potential

$$V(r) = k(R-r)^3, \quad r \leq R \tag{1}$$

where r is the distance between the atom and the center of the indenter; for r > R, the force vanishes. The force constant amounts to k = 11.7 eV/Å ^{3} [39].

In the simulations, we use periodic boundary conditions in the lateral directions while the top surface is left free. The calculations are performed using the open-source code LAMMPS [45]. The Crystal Analysis Tool (CAT) [46–48] is used to identify dislocations and stacking faults. OVITO [49] is employed to visualize the simulation results.

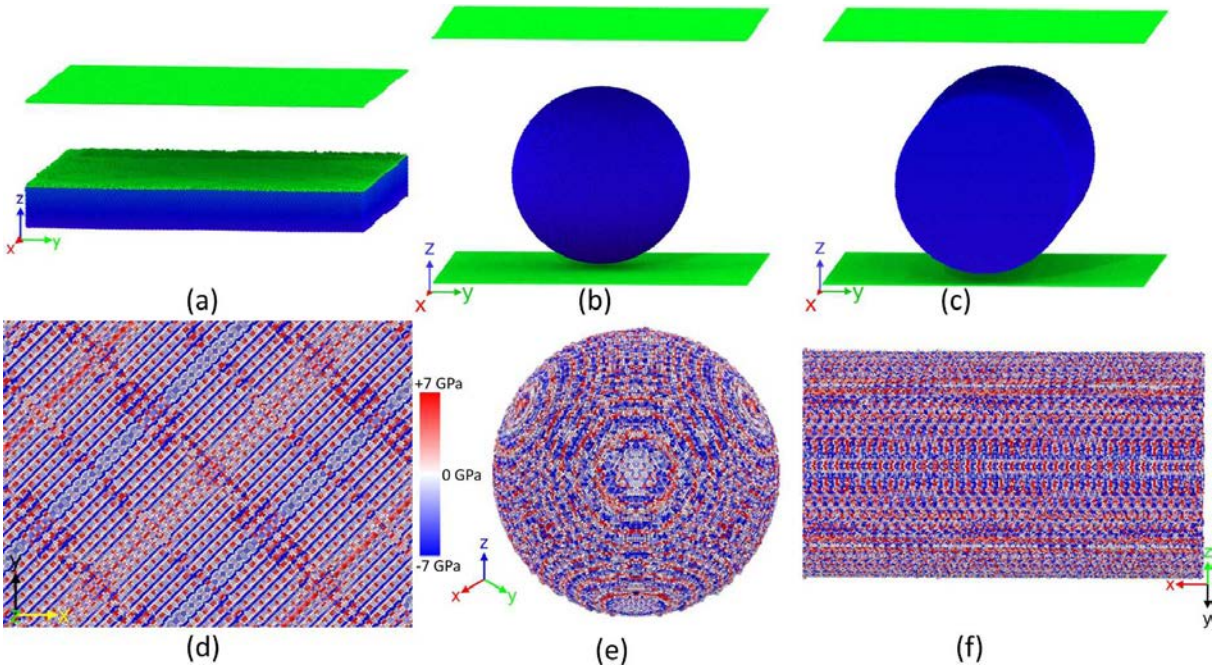

Figure 1: The three systems studied: (a) plate reinforcement, (b) spherical particle, (c) cylindrical fiber. Only surface atoms are shown. Green: Al. Blue: Si. (d)–(f) show the Al side of the interfaces where atoms are colored by their local hydrostatic stress, see color bar included in (e).

3 RESULTS

In the following we discuss how the dislocations generated by the indentation in the Al matrix interact with the Si reinforcement. The typical features will be analyzed by considering in detail representative cases for each of the three shapes studied here.

3.1 Plate

In the plate reinforcement, we observe dislocation emission from the plate, Figs. 2(a)–(d), and reactions with subsequent dislocations emitted from the indentation area leading to work hardening of the material, (e)–(i). In (a), a dislocation loop approaches the plate and more than half of it sinks into it (b). A small dislocation is emitted nearby (c) (marked by an arrow) and grows (d); its Burgers vector is different from that of the original loop as shown in top left inserted graph in (d). Note that the region of the interface where this happens is of roughly square shape and characterized by a consistently strong compressive stress, as seen in the top middle inserted graph (d).

In (e), the emitted dislocation continues growing rapidly and almost touches a second dislocation loop that was emitted from the indentation area; at the same time the high-stress zone on the interface is reduced in size and the first loop shrinks again. The high-stress zone and the gliding of the second loop into the plate lead to the strong growth of the emitted dislocation.

The emitted dislocation interacts with the left part of the second loop (f), forming a dislocation cluster with three terminals on the interface, denoted as T1–3 in the following. In (g)–(i) we analyze in detail the evolution of these dislocations. T1 moves — together with the second loop – away from the center of the indentation area (g), while the dislocation bounded by T3 moves upward (h) and reaches the center of the indentation area (i). Thus, the left part of the second loop and the emitted dislocation play a dominant role in the evolution of T1 and T3, respectively.

This scenario demonstrates that the interaction of the indentation-induced plasticity with the interface does not simply reflect dislocations; rather they change their glide direction and may move back towards the indentation zone, where they may contribute to work hardening of the material. Zones of high compressive stress formed on the interface are crucial in the process of dislocation emission.

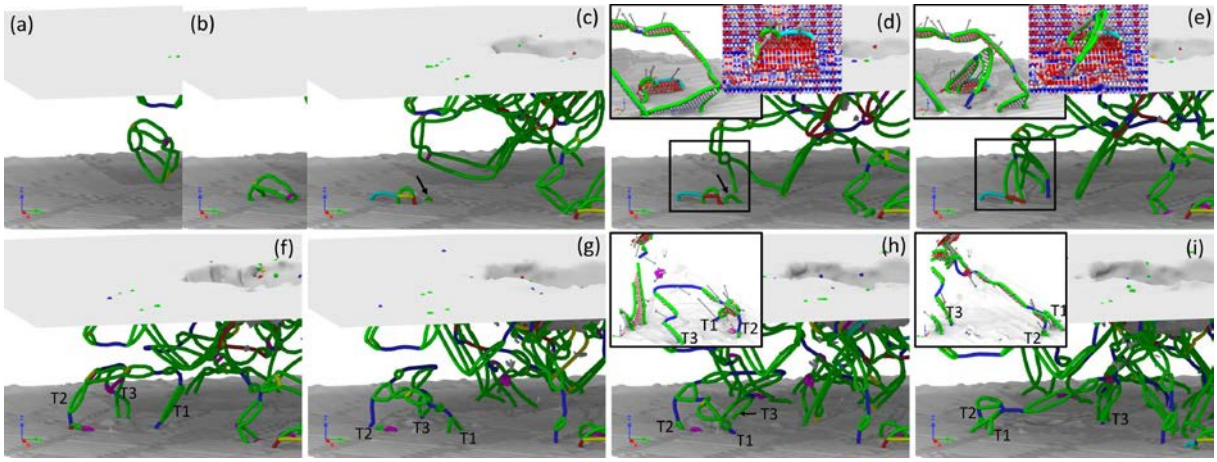

Figure 2: Processes occurring in plate-reinforced MMC at indentation depths of 20 °A (a), 21 °A (b), 31 °A (c), 32 °A (d), 33 °A(e), 34 °A (f), 43 °A (g), 45 °A (h) and 47 °A (i). Only defects (dislocations, interface) are shown. Lines denote dislocation lines with Burgers vector 1/2 <110> (dark blue), 1/6 <112> (green), 1/6 <110> (purple), 1/3 <111> (light blue) and 1/3 <100> (yellow). Red lines denote other dislocations. The arrow in (c) highlights a dislocation emitted from the interface. Inserts in (d) and (e) zoom into the areas highlighted by the rectangle; the top middle inserts color atoms by their local hydrostatic stress, see color bar in Fig. 1(e). Subpanels (f)–(i) follow the evolution of dislocations with terminal ends on the interface denoted by T1–3. The inserts in (h) and (i) zoom into the terminal movements.

3.2 Particle

Figs. 3(a)–(h) display the evolution of plasticity in the particle-reinforced MMC. Induced by the indentation, dislocations are formed beneath the indenter (a). As shown in previous simulations of indentation into Al [50–52], a dislocation loop forms and is ejected from the high-stress region into the

substrate (a). Atoms inside the loop show compressive hydrostatic stress while those around the loop exhibit tensile values.

The original glide direction of the loop (a) does not cross the reinforcement. However, because of the strong stress field in the vicinity of the particle, the bottom part of the loop (which is closer to the particle) slows down while the top part continues moving with its original speed. Thus, the loop starts rotating and hence changes its glide direction (b). Later, the bottom part of the loop approaches the particle more closely and is repelled, resulting in another loop re-orientation, and the loop almost recovers its original shape and glide direction (c).

The fate of another loop approaching the particle is shown in (d–h). This loop touches the particle (d) at a position of local compressive stress (e), which compensates the tensile pressure outside the loop. In the stress field exerted by the indentation, the loop breaks up creating two terminal points (f) on the particle surface. The interaction reduces the elastic energy, since now the inside of the loop (compressive pressure) comes into contact with regions of the particle surface under tensile pressure (f). The terminal points glide on the particle surface (g) until the loop is released from the particle and moves away from the indentation region (h). Note that just before a loop terminal gets released from the particle – e.g., the left terminal in (f) – its stress state changes from compressive to tensile; this signals the ejection of the dislocation from the particle.

We conclude that spherical particles exert an influence on the glide direction of nearby dislocations. However, no final absorption of dislocations in the particle was observed.

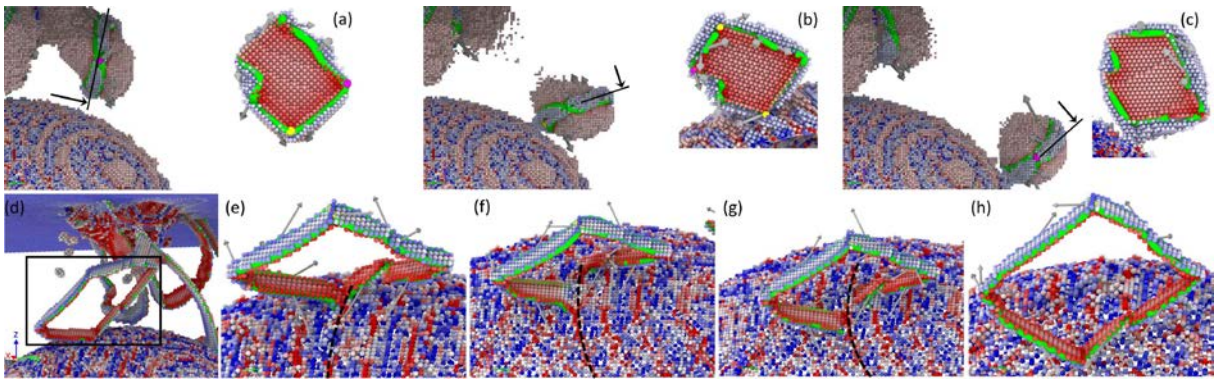

Figure 3: Processes occurring in particle-reinforced MMC at indentation depths of 15 °A (a), 16 °A (b) and 17 °A (c), 29 °A (d), 30 °A (e), 34 °A (f), 35 °A (g) and 37 °A (h). In subpanels (a)–(c), only atoms with stress outside the window (−1,+1) GPa are shown; in subpanels (d)–(h), only defects (surface, interface, stacking faults, dislocations) are shown. Atoms are colored by local hydrostatic stress, see color bar in Fig. 1(e). Dislocation lines are colored as in Fig. 2. Inserts in (a)–(c) show a slice (black line) through the plastic zone along the arrow direction. The black rectangle in (d) highlights the dislocation loop whose evolution is followed in (e)–(h). Dashed circle in (e)–(f) follows a high-stress ring on the reinforcement.

3.3 Fiber

The processes occurring at a fiber reinforcement are displayed in Figs. 4(a)–(i). In (a)–(c), a dislocation gradually sinks into the fiber, similar to our findings for the plate reinforcement. On the other side, we also observe processes, where a dislocation loop bypasses the fiber (d–e), similar to what we observed for a particle reinforcement. Finally, the interface may emit a dislocation (g–h), similar to our findings for the plate reinforcement.

However, the first dislocation is eventually completely swallowed by the interface (c), and the emitted dislocation (h) disappears (i) instead of growing and moving to the center of indentation area. These two observations are in contrast to our findings for the plate. We argue that high-stress zones, such as the one we identified for the plate, cannot form on the fiber because of its cylindrical shape, where the high stress, resulting locally from dislocations gliding into the interface, can easily be distributed on the surface. Thus, the dislocations can sink in entirely and the emitted dislocation is absorbed again.

Thus the interaction of dislocations with a fiber reinforcement confirms our findings about strengthening and toughening mechanisms in particle and plate reinforcements. Dislocations meeting the fiber with a glide direction along the fiber axis behave similar to the plate scenario, while dislocations moving in a direction perpendicular to the fiber axis behave similar to the particle scenario. We conclude that the local curvature of the reinforcement governs the behavior of the dislocation.

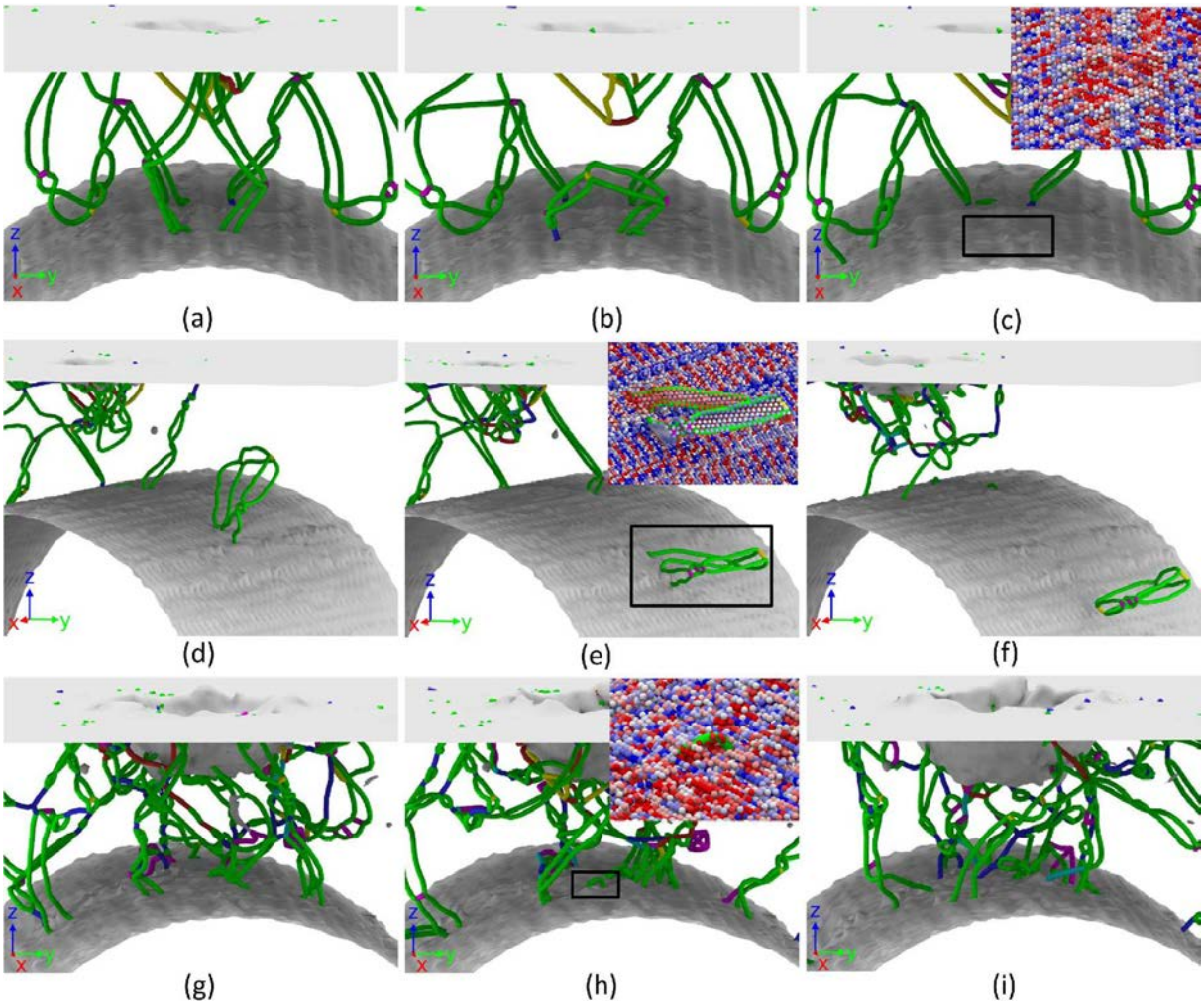

Figure 4: Processes occurring in fiber-reinforced MMC at indentation depths of 20 °A (a), 20.5 °A (b), 21 °A (c), 24 °A (d), 24.5 °A (e) 25 °A (f), 42 °A (g), 45 °A (h) and 48 °A (i). Only defects (surface, interface, dislocations) are shown. Inserts in (c), (e) and (h) zoom into the areas highlighted by the rectangles. Atoms are colored by local hydrostatic stress, and lines denote dislocation lines as in Fig. 2. The rectangle in (h) marks a dislocation emitted from the reinforcement.

4 SUMMARY

Atomistic simulation allowed us to study in detail the generation of plasticity and the mobility of defects during nanoindentation of an Al/Si MMC. Dislocation emission from the reinforcements is found most prominently for the plate geometry, less pronouncedly for the fiber and not at all for the sphere. This demonstrates that the curvature of the reinforcement plays an important role in strengthening and toughening mechanisms of MMCs. Plate-reinforced MMC excels in its performance during deformation by the formation of high-stress zones that particle and fiber reinforcements cannot attain. Interestingly, plates can emit dislocations back into the indentation area, leading to high strain hardening at low strain values as well as high strength; this feature is corroborated by experiment [16].

On the other hand, plate reinforcements can emit dislocations with gliding directions different from those approaching the plate and thus stimulate more slip planes and slip directions, enhancing overall ductility in the matrix.

In detail the three different shapes of the ceramic reinforcement studied here exhibited the following features in their interaction with dislocations.

1. Plate reinforcements act directly by annihilating Al dislocations loops at the interface; they are emitted later, and possibly in another direction. The formation of high-stress zones on the interface is crucial for this phenomenon; they are formed by the absorption of dislocations and disappear after re-emitting another dislocation. Since the emitted dislocations may glide back to the indentation area and interact with the plasticity there, plate reinforcements will strengthen the composite. On the other hand, since more slip systems may be activated by the emission of dislocations from the interface, enhanced ductility may be expected.

2. Reinforcements with spherical particles hinder the mobility of dislocations in the metal. Two effects are responsible for this: (i) the ceramic influences the direction of motion of the dislocations; (ii) the interface swallows part of the Al dislocations that approach the interface.

3. Fiber reinforcements show a behavior in between that of the sphere and the plate. According to their geometry they behave similar to a spherical particle for dislocations approaching vertical to the fiber axis, and similar to a plate for dislocations approaching along the fiber axis. However, we observed no sizable dislocation emission since no high-stress zone formed in the interface due to its curved shape.

We conclude that the shape of the reinforcement plays a dominant role in the mechanisms underlying the strengthening of the MMC. This feature is of prime interest when tailoring the mechanical properties of any material strengthened by a hard phase as well as for MMCs.

ACKNOWLEDGEMENTS

Simulations were performed at the High Performance Cluster Elwetritsch (RHRK, TU Kaiserslautern, Germany). We acknowledge the financial support of the Deutsche Forschungsgemeinschaft via the IRTG 2057.

REFERENCES

[1] N. Chawla and K. K. Chawla, Metal Matrix Composites (Springer, New York, 2013), 2nd ed.
[2] A. F. Boostani, S. Tahamtan, Z. Y. Jiang, D. Wei, S. Yazdani, R. A. Khosroshahi, R. T. Mousavian, J. Xu, X. Zhang, and D. Gong, Compos. Part A: Appl. S. 68, 155 (2015).
[3] F. Mokdad, D. L. Chen, Z. Y. Liu, B. L. Xiao, D. R. Ni, and Z. Y. Ma, Carbon 104, 64 (2016).
[4] T. Wang, Y. Zheng, Z. Chen, Y. Zhao, and H. Kang, Mater. Design 64, 185 (2014).
[5] C. Koch, Scr. Mater. 49, 657 (2003).
[6] E. Ma, Scr. Mater. 49, 663 (2003).
[7] H. A. Hassan and J. J. Lewandowski, Scr. Mater. 61, 1072 (2009).
[8] L. Jiang, Z. Li, G. Fan, and D. Zhang, Scr. Mater. 65, 412 (2011).
[9] L. Jiang, H. Yang, J. K. Yee, X. Mo, T. Topping, E. J. Lavernia, and J. M. Schoenung, Acta Mater. 103, 128 (2016).
[10] Y.-H. Li, W. Housten, Y. Zhao, and Y. Q. Zhu, Nanotechnology 18, 205607 (2007).
[11] T. J. Kang, J.-W. Yoon, D.-I. Kim, S. S. Kum, Y.-H. Huh, J.-H. Hahn, S. H. Moon, H.-Y. Lee, and Y. H. Kim, Adv.Mater. 19, 427 (2007).
[12] L. Jiang, Z. Li, G. Fan, L. Cao, and D. Zhang, Scr. Mater. 66, 331 (2012).
[13] C. Lee, X. Wei, J. W. Kysar, and J. Hone, Science 321, 385 (2008).
[14] J. Wang, Z. Li, G. Fan, H. Pan, Z. Chen, and D. Zhang, Scr. Mater. 66, 594 (2012).
[15] Y. Kim, J. Lee, M. S. Yeom, J. W. Shin, H. Kim, Y. Cui, J. W. Kysar, J. Hone, Y. Jung, S. Jeon, et al., Nat. Commun. 4, 2114 (2014).
[16] Z. Li, Q. Guo, Z. Li, G. Fan, D.-B. Xiong, Y. Su, J. Zhang, and D. Zhang, Nano Lett. 15, 8077 (2015).
[17] Z. Li, L. Zhao, Q. Guo, Z. Li, G. Fan, C. Guo, and D. Zhang, Scr. Mater. 131, 67 (2017).

[18] S. Feng, Q. Guo, Z. Li, G. Fan, Z. Li, D.-B. Xiong, Y. Su, Z. Tan, J. Zhang, and D. Zhang, Acta Mater. 125, 98 (2017).
[19] L. Jiang, T. Hu, H. Yang, D. Zhang, T. Topping, E. J. Lavernia, and J. M. Schoenung, Nanoscale 8, 10541 (2016).
[20] A. C. Fischer-Cripps, Nanoindentation (Springer, New York, 2004), 2nd ed.
[21] A. Gouldstone, N. Chollacoop, M. Dao, J. Li, A. M. Minor, and Y.-L. Shen, Acta Mater. 55, 4015 (2007).
[22] S. Bhattacharya, A. R. Riahi, and A. T. Alpas, Mat. Sci. Eng. A 527, 387 (2009).
[23] S. Xia, Y. Qi, T. Perry, and K.-S. Kim, Acta Mater. 57, 695 (2009).
[24] Z. Yuan, F. Li, P. Zhang, B. Chen, and F. Xue, Chinese Journal of Aeronautics 27, 397 (2014).
[25] Z. Yuan, F. Li, P. Zhang, B. Chen, F. Xue, and M. Z. Hussain, J. Mater. Res. 29, 586 (2014).
[26] D. K. Ward, W. A. Curtin, and Y. Qi, Acta Mater. 54, 4441 (2006).
[27] D. K. Ward, W. A. Curtin, and Y. Qi, Compos. Sci. Technol. 66, 1151 (2006).
[28] M. R. Rosenberger, E. Forlerer, and C. E. Schvezov, Mat. Sci. Eng. A 463, 275 (2007).
[29] J. F. Su, X. Nie, and V. Stoilov, Mat. Sci. Eng. A 527, 7168 (2010).
[30] I. Szlufarska, Mater. Today 9, 42 (2006).
[31] C. Lu, Y. Gao, G. Michal, G. Deng, N. N. Huynh, H. Zhu, X. Liu, and A. K. Tieu, J. Nanosci. Nanotechnol. 9, 7307 (2009).
[32] G. Ziegenhain and H. M. Urbassek, Philos. Mag. 89, 2225 (2009).
[33] G. Ziegenhain, A. Hartmaier, and H. M. Urbassek, J. Mech. Phys. Sol. 57, 1514 (2009).
[34] G. Ziegenhain, H. M. Urbassek, and A. Hartmaier, J. Appl. Phys. 107, 061807 (2010).
[35] Y. Gao, C. J. Ruestes, and H. M. Urbassek, Comput. Mater. Sci. 90, 232 (2014).
[36] Y. Gao, C. J. Ruestes, D. R. Tramontina, and H. M. Urbassek, J. Mech. Phys. Sol. 75, 58 (2015).
[37] I. Alabd Alhafez, C. J. Ruestes, Y. Gao, and H. M. Urbassek, Nanotechnology 27, 045706 (2016).
[38] D. E. Kim and S. I. Oh, J. Appl. Phys. 104, 013502 (2008).
[39] Z. Zhang, A. Stukowski, and H. M. Urbassek, Comput. Mater. Sci. 119, 82 (2016).
[40] A. Noreyan, Y. Qi, and V. Stoilov, Acta Mater. 56, 3461 (2008).
[41] P. Saidi, T. Frolov, J. J. Hoyt, and M. Asta, Model. Simul. Mater. Sci. Eng. 22, 055010 (2014).
[42] F. H. Stillinger and T. A. Weber, Phys. Rev. B 31, 5262 (1985).
[43] M. I. Mendelev, M. J. Kramer, C. A. Becker, and M. Asta, Philos. Mag. 88, 1723 (2008).
[44] C. L. Kelchner, S. J. Plimpton, and J. C. Hamilton, Phys. Rev. B 58, 11085 (1998).
[45] S. Plimpton, J. Comput. Phys. 117, 1 (1995), http://lammps.sandia.gov/.
[46] A. Stukowski, V. V. Bulatov, and A. Arsenlis, Model. Simul. Mater. Sci. Eng. 20, 085007 (2012).
[47] A. Stukowski, Model. Simul. Mater. Sci. Eng. 20, 045021 (2012).
[48] A. Stukowski and A. Arsenlis, Model. Simul. Mater. Sci. Eng. 20, 035012 (2012).
[49] A. Stukowski, Model. Simul. Mater. Sci. Eng. 18, 015012 (2010), http://www.ovito.org/.
[50] K. J. Van Vliet, J. Li, T. Zhu, S. Yip, and S. Suresh, Phys. Rev. B 67, 104105 (2003).
[51] Y. Lee, J. Y. Park, S. Y. Kim, S. Jun, and S. Im, Mech. Mater. 37, 1035 (2005). 6
[52] C. J. Ruestes, E. M. Bringa, Y. Gao, and H. M. Urbassek, in Applied Nanoindentation in Advanced Materials, edited by A. Tiwari and S. Natarajan (Wiley, 2017), chap. 14, p. 315.